Excitation functions and asymmetric fission barriers for intermediate mass fragments: 486–730 MeV ^{86}Kr + ^{63}Cu

J. Boger* and John M. Alexander

Department of Chemistry, State University of New York at Stony Brook, Stony Brook, New York 11794
(Received 17 November 1993)

Fragments with $4 \leq Z \leq 15$ have been studied from the reaction 486, 550, 640, and 730 MeV ^{86}Kr+^{63}Cu. A standard analysis procedure has been used to characterize the associated asymmetric fission barriers and compare them to the Sierk model (Yukawa plus exponential finite range nuclear potential). The predicted YEFRN model barriers are too small by $\approx$37%, a result that is in contrast with other studies. The often used statistical model code GEMINI also fails to account for these excitation functions.

PACS number(s): 24.60.Dr, 25.70.Gh, 25.70.Jj

I. INTRODUCTION

Intermediate mass fragments (IMF) have been intensively investigated for clues to their production mechanism, e.g., their charge distributions, excitation functions, kinetic energies, and angular distributions. A picture is now emerging that several processes are responsible. At low to intermediate energies, the major mechanisms are projectile-fragment breakup (from peripheral collisions) and asymmetric binary-fission-like breakup (from central collisions) (e.g., [1,2]). As incident energies increase, the importance of three- or more body breakup increases [3], and at even higher energies, multifragment emission results in very high IMF multiplicities [4].

In previous work we have shown that the predominant mode of IMF production for the ^{86}Kr + ^{63}Cu reaction (incident energies $E/A \leq 10$ MeV) is essentially binary-fission-like breakup (>95%) of a completely fused nucleus (e.g., [2,5]) with little contribution from sequential or multifragment emission (<5%). Similar observations have been made by other authors [6,7] for reactions in this energy regime. Additionally, IMF excitation functions have been studied in the attempt to derive semi-empirical asymmetric fission barriers (see, for example, [8,9]). This interest stems from a desire to test (and/or refine the parameters in) current forms of the macroscopic nuclear model. The Sierk formulation predicts asymmetric fission barriers calculated with a Yukawa plus exponential finite range nuclear (YEFRN) potential [10,11]. In this paper we follow this path [8–12] by analyzing excitation functions for IMF's from the reaction ^{86}Kr + ^{63}Cu.

The statistical model framework is used in a simple form with an analytical formulation for the IMF branching ratio. This approach, as outlined in Sec. II, follows closely that of [9] with the use of some additional empirical information on the production of light charged

particles. In Sec. III, values for the emission barriers are derived from fits to the IMF excitation functions for $4 \leq Z_{\text{IMF}} \leq 14$. These extracted barriers are compared to barrier values predicted by the YEFRN model [10,11,13]. In Sec. IV we examine the assumptions that were made in formulating the analytical expressions. Our conclusions are summarized in Sec. V. We find that this overall approach does not lead to a satisfying description of the IMF barriers. Either the YEFRN predictions (e.g., the empirical parameters of the model) are inadequate or the standard procedure from [9] is inadequate. In addition the excitation functions are not well described by the code GEMINI [7], a more detailed implementation of the same physical model.

II. THE STATISTICAL MODEL AND ASYMMETRIC FISSION BARRIERS

In order to extract saddle-point potential barriers that may be compared with macroscopic calculations, we begin by examining standard formulas for the IMF branching ratio from the statistical model. This analysis closely follows [9] and [14]; its approximations are reassessed in Sec. IV below.

The cross section for producing an IMF from an emitter nucleus at a given excitation energy E^* may be written

$$\sigma_{\text{IMF}}(E^*) = \sigma_{CN} \frac{\Gamma_{\text{IMF}}(E^*)}{\Gamma_{\text{tot}}(E^*)} \qquad (2.1)$$

where σ_{CN} is the cross section for complete fusion, $\Gamma_{\text{IMF}}(E^*)$ is the partial width for the production of the IMF (of specific Z_{IMF}), and $\Gamma_{\text{tot}}(E^*)$ is the total decay width. The total width is the sum of partial widths

$$\Gamma_{\text{tot}}(E^*) \approx \Gamma_n(E^*) + \Gamma_p(E^*) + \Gamma_\alpha(E^*) + \sum_{Z=3}^{Z_{\text{max}}} \Gamma_{\text{IMF}}(E^*),$$
$$\qquad (2.2)$$

*Present address: Texas A&M University, Cyclotron Institute, College Station, TX 77843-3366.

where subscripts n, p, and α refer to neutrons, protons, and alpha particles. The summation includes the heavier fragments, such as the IMF's and fission fragments. The factor $\Gamma_{\text{IMF}}(E^*)/\Gamma_{\text{tot}}(E^*)$ is therefore the branching ratio or the probability for the ejection of an IMF of given Z from a given composite nucleus with excitation energy E^*.

Following the examples of both [9] and [14], one may use the statistical model to write the partial width for a fission channel (excluding for the moment any spin dependence)

$$\Gamma_f = \frac{1}{2\pi\rho_0(E_0^*)} \int_0^{E_0^* - B_{\text{fiss}}^{CN}} \rho(E_0^* - B_{\text{fiss}}^{CN} - \epsilon_f) d\epsilon_f, \tag{2.3}$$

where ρ_0 is the level density of the parent nucleus, E_0^* is its gross excitation energy and B_{fiss}^{CN} is the potential barrier height for that channel with respect to the ground state of the parent nucleus, ϵ_f is the kinetic energy of separation at the saddle point, and the integral is made over the level density ρ at the saddle point. Equation (2.3) is based on the so-called transition-state model. Within the framework of this model, the probability for the emission of a fragment is decided at the saddle-point. Differences in saddle-point barriers control the relative yields, and detailed properties of the final fragments are not relevant. Macroscopic model calculations have been made for the saddle-point barriers and shapes as a function of both mass asymmetry and angular momentum [13]. Use of these values in Eqs. (2.1)–(2.3) can give predictions for $\Gamma_{\text{IMF}}/\Gamma_{\text{tot}}$ and σ_{IMF}. Or, as in [9], one may use the excitation functions for given IMF's to extract their associated fission barriers for comparison to model predictions.

The partial width for neutron emission is also given by the statistical model

$$\Gamma_n = \frac{2mR^2g}{\hbar^2 2\pi\rho(E_0^*)} \int_0^{E_0^* - B_n} \epsilon_n \rho_D(E_0^* - B_n - \epsilon_n) d\epsilon_n, \tag{2.4}$$

where m is the mass of the neutron, R is the radius of the daughter nucleus, B_n is the binding energy of the neutron, ϵ_n is its kinetic energy, g is the intrinsic spin degeneracy of the neutron, and the integral is made over the level density ρ_D of the residual or daughter nucleus after the emission of a neutron from the parent nucleus. Equation (2.4) is based on the so-called statistical evaporation model. Within the framework of this model, the phase space of the daughter nucleus determines the exit channel probability. This is the fundamental difference between the transition-state and statistical evaporation models. With some simple approximations [14] this expression has been used [9] to obtain an analytical form for the branching ratio needed for use in Eq. (2.1).

For the ^{149}Tb* composite nucleus, previous work indicates that the spin range $(0\hbar-75\hbar)$ leads to heavy fragment residues [i.e., evaporation residues (ER)] and that this reaction class is the source of light IMF emission

[1,15]. Kinematical calculations have been made of the recoil given to a heavy nuclear partner by the emission of H, He, Li, Be, and other IMF's. It is clear that emission of the lighter IMF's ($_3$Li, $_4$Be,...) gives a relatively small recoil and would leave the heavy nuclear partner in the ER reaction class. It is also clear that emission of the heavier IMF's ($_{15}$P, $_{14}$Si,...) gives a much larger recoil and would leave the heavy nuclear partner in the fusion-fission reaction class. The probability is low for emitting two IMF's or for any form of ternary fission in this energy domain [2]. Therefore, light particle production (n, H, and He) is the major competitor with IMF production. Furthermore, the Z distributions for the reactions 486, 550, 640, and 730 MeV ^{86}Kr + ^{63}Cu show that the cross sections for the production of the light IMF's are two to three orders of magnitude less than those for light particles [1]. Equation (2.2) may therefore be approximated as follows

$$\Gamma_{\text{tot}}(E^*) \approx \Gamma_n(E^*) + \Gamma_p(E^*) + \Gamma_\alpha(E^*). \tag{2.5}$$

The next approximation involves the relationship between Γ_{tot} and Γ_n. This may be obtained from the experimental light-charged particle multiplicities and the associated energy balance. We have calculated by the method of [16] the ratio of neutron to ^{4}He multiplicities, which was then normalized to the experimental ^{4}He multiplicity, in order to estimate the unmeasured neutron multiplicity. According to these estimates made for the excitation energy range 128–231 MeV, neutron emission comprises a nearly constant 75% of the total light particle multiplicity and therefore about 75% of the total decay width. (No correction for alpha particle evaporation was made in [9].) We may then write

$$\Gamma_{\text{tot}}(E^*) \approx \frac{\Gamma_n(E^*)}{0.75}, \tag{2.6}$$

where the purpose of this approximation is evident with respect to Eq. (2.1). The branching ratio for fissionlike production of an IMF is now written

$$\frac{\Gamma_{\text{IMF}}(E^*)}{\Gamma_{\text{tot}}(E^*)} = \frac{0.75\Gamma_f(E^*)}{\Gamma_n(E^*)}. \tag{2.7}$$

The energy of rotation may be included (following [9]) to incorporate a simple spin dependence in the branching ratio. This is done in Eq. (2.8) by subtracting the rotational energy of the saddle-point nucleus in the calculation of the maximum thermal excitation energy at the saddle point E_{sp}^*. For the saddle-point nucleus this means

$$E_{\text{sp}}^* = E_0^* - E_{\text{rot,sp}} - B_{\text{fiss}}^{CN} \tag{2.8}$$

where its rotational energy is

$$E_{\text{rot,sp}} = \frac{\hbar^2 J^2}{2\Im_{\text{sp}}}. \tag{2.9}$$

Similarly for the daughter nucleus we use the subscript D,

$$E_D^* = E_0^* - E_{\text{rot},D} - B_n, \tag{2.10}$$

where its rotational energy is

$$E_{\text{rot},D} = \frac{\hbar^2 J^2}{2\Im_D} \qquad (2.11)$$

with $\Im_{\text{sp}}$ ($\Im_D$) the moment of inertia of the saddle-point (daughter) nucleus. These moments of inertia may be obtained from predictions of the YEFRN model [13], but as shown below there is not much sensitivity to the means used for estimating $\Im_{sp}$ and $\Im_D$.

Inclusion of Eqs. (2.8)–(2.11) in Eq. (2.7) allows for a simple summation over spin for $J = 0 - J_{\text{max}}$ so that spin-dependent branching ratios may be computed for each excitation energy. Figure 1 shows the calculated dependence of the branching ratio on spin for the production of $Z = 6$ from a composite nucleus with an initial excitation energy of 194 MeV. Only first-chance IMF emission and competition with light particles are considered in this figure. We see that IMF production becomes increasingly competitive with light particle production as the spin of the emitter increases. This is because the fission barriers, as calculated by the model, decrease with increasing spin [13].

Of course symmetric fission also takes place so the role of fission competition must also be included. Using the equations above we sketch out the qualitative results of the statistical model and display them as the predicted spin dependence for three competitive decay processes. Figure 2 gives their branching ratios, $\Gamma_i/\Gamma_{\text{tot}}$: (1) light particle production ($\Gamma_{np\alpha}/\Gamma_{\text{tot}}$); (2) IMF production specifically for $Z = 5$($\Gamma_{\text{IMF}}/\Gamma_{\text{tot}}$); and (3) symmetric fission ($\Gamma_{\text{fiss}}/\Gamma_{\text{tot}}$), where

$$\Gamma_{\text{tot}} = \Gamma_{np\alpha} + \Gamma_{\text{fiss}} + \Gamma_{\text{IMF}}. \qquad (2.12)$$

Only first-chance IMF emission is included.
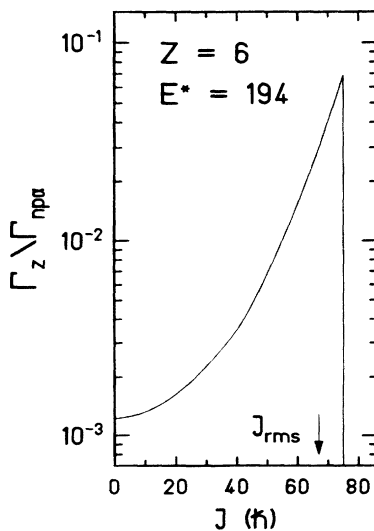
Clearly in this calculation light particle production

FIG. 1. Branching ratio for carbon as a function of the angular momentum J of the ^{149}Tb* ($E^* = 194$ MeV) compound nucleus. The arrow indicates the J_{rms} value of the emitter for this sharp cutoff approximation.
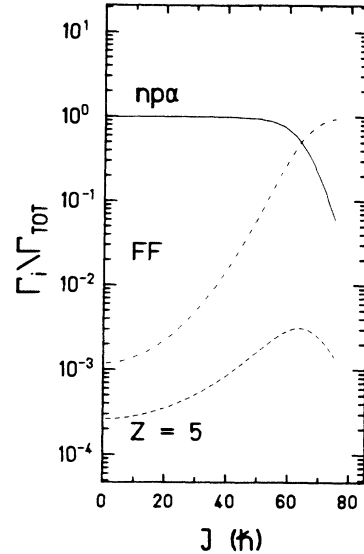

FIG. 2. Comparison of branching ratios for light particle production ($\Gamma_{np\alpha}/\Gamma_{\text{tot}}$), fission ($\Gamma_{\text{fiss}}/\Gamma_{\text{tot}}$), and IMF production for $Z_{\text{IMF}} = 5$ ($\Gamma_{\text{IMF}}/\Gamma_{\text{tot}}$). These calculated first-chance emission branching ratios are based on Eqs. (2.1)–(2.12). Here Γ_{tot} includes the partial width for symmetric fission.

(indicated by subscript $np\alpha$) dominates the spin region $0 < J < 60$; then fission (subscript fiss) begins to take over as the preferred decay path. According to these calculations, the IMF's are produced in a rather high-spin region where light particle production has diminished and symmetric fission has begun to increase in importance but has not yet assumed heavy domination. This is shown by the dotted line in Fig. 2. At sufficiently high spins, the IMF's cannot compete with fission decays to high Z fragments, so that the branching ratio for IMF production reaches a maximum and then declines. In the sharp cutoff approximation (Fig. 1) one hopes, as usual, to compensate for omission of some IMF production from the tail at high spin (Fig. 2) by some over-prediction for $J \lesssim J_{\text{max}}$. The virtue of using the empirical value of J_{max} is that it imposes a correct representation of the results of ER-fission competition with no model dependence. Therefore, our calculations include fission competition implicitly by using the empirical value of J_{max}.

These qualitative trends with spin are also predicted by the more detailed statistical model calculations of GEMINI [7]. Figure 3 is a plot of the first-chance branching ratios for light particle production (solid line), complex fragment production (i.e., $Z \geq 3$) (dashed line), and for the emission of an IMF of $Z = 5$ (dash-dotted line). Similar to the trend shown in Fig. 2, light particle production dominates the exit channel phase space for the spin region $0 \leq J \leq 75\hbar$, whereupon high Z fragment production (or fission) becomes the most competitive decay path. The branching ratios for the production of $Z = 5$ are also similar; its competitiveness increases with spin as the branching ratio for light particle production declines. For larger spins, the branching ratio for $Z = 5$ peaks then declines as more mass symmetric fission dominates the largest spins.
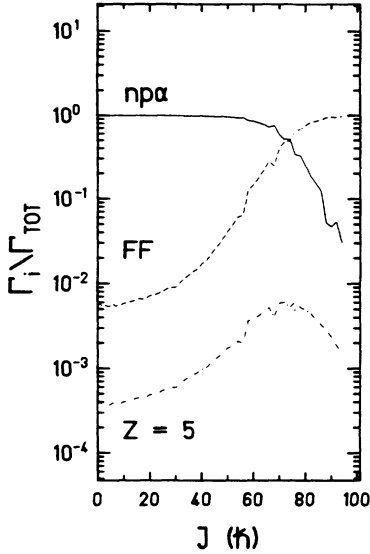
FIG. 3. Comparison of branching ratios calculated by GEMINI for first chance emission of light particles, fission, and $Z_{\mathrm{IMF}} = 5$.

Detailed differences in the spin dependence of the calculated branching ratios shown in Figs. 2 and 3 [i.e., from Eq. (2.1) and from GEMINI] result from a host of different approximations that are hard to trace. GEMINI is capable of more sophisticated calculations than the simple formulation of Eqs. (2.1)–(2.12). Nonetheless, the similarities between these two calculations give confidence in qualitative features of the spin dependence as derived from the simple form of the statistical model used in Ref. [9] and below.

The advantage of Eqs. (2.6)–(2.12) is that one can include empirical information for charged particle and ER production in a simple and transparent way and thus avoid hidden complexities that may be imbedded in the less flexible formulation of a complex computer code; a disadvantage lies in the possible oversimplification of the spin dependence. We proceed with Eqs. (2.1)–(2.12) so that the results for this study of the system ^{149}Tb* can be directly related to those for ^{75}Br* from [9].

III. ASYMMETRIC FISSION BARRIERS AND IMF YIELDS

To generate IMF excitation functions using Eq. (2.1), we select a value for the level density parameter of $a_n = A/10$. The spin range employed is $J = 0\hbar$–$75\hbar$, which corresponds to the ER reaction class [17]. Individual spin-dependent branching ratios are computed for each value of J; they are then summed and weighted to obtain the IMF branching for each excitation energy. These calculated excitation functions may be fitted to the experimental IMF excitation functions in the usual way by adjusting two free parameters, a_f/a_n and B_{fiss}^{CN}. The derived values of B_{fiss}^{CN} may then be compared to YEFRN model predictions. It is more revealing to give the ratio

of level density parameters, a_f/a_n, as this gives insight into the phase space available to the saddle-point nucleus compared to that for the daughter nucleus. A more deformed saddle-point nucleus is expected to have more degrees of freedom than a more nearly spherical daughter nucleus; one therefore expects to find $a_f/a_n > 1$ [18].

We first calculate IMF excitation functions and assume no prefission evaporation of light particles. We further assume that the moments of inertia used in these calculations are independent of spin. That is, the moments of inertia for the saddle-point and daughter nuclei are evaluated for $J = 0$. This is done as a simple first step in the calculation as well as to limit the dependence on the YEFRN model. These assumptions will be addressed later. Values of J_{rms} are also extracted from the same parametrization used to fit the excitation functions

$$J_{\mathrm{rms}} = \left\{ \frac{\sum_{J=0}^{75}(2J+1)\left(\frac{\Gamma_{\mathrm{IMF}}}{\Gamma_{\mathrm{tot}}}\right)J^2}{\sum_{J=0}^{75}(2J+1)\left(\frac{\Gamma_{\mathrm{IMF}}}{\Gamma_{\mathrm{tot}}}\right)} \right\}^{1/2}. \quad (3.1)$$

Figure 4 shows the calculated fits to the IMF excitation functions; these calculated excitation functions match the measured ones very well. Similar fits were made for IMF's up to $Z = 14$. Table I lists the derived values for barriers (B_{fiss}^{CN}), level density parameter ratios (a_f/a_n), and J_{rms} for each IMF under the column headed "Fixed $\Im$." A more refined analysis (discussed in Sec. IV) has also been done that includes the calculated dependence of $\Im$ on spin. Results are given in Table I under the column headed "Spin-dependent $\Im$." Figure 5 shows these barrier values (open circles) and those from the YEFRN model (lower curve) and rotating liquid drop model (RLDM) (upper curve) as functions of the mass asymmetry parameter η, where

$$\eta = \frac{A_{\mathrm{HF}} - A_{\mathrm{IMF}}}{A_{\mathrm{HF}} + A_{\mathrm{IMF}}}. \quad (3.2)$$
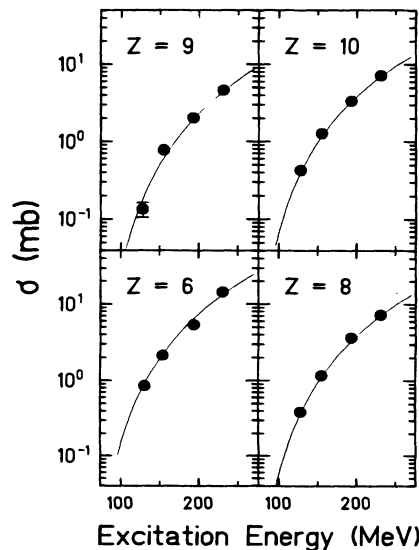

FIG. 4. Excitation functions for $Z_{\mathrm{IMF}} = 6, 8, 9$, and 10. Experimental data points are the solid circles. The smooth curves are theoretical fits based on Eqs. (2.1)–(2.12) and first-chance fission.

TABLE I. Derived asymmetric fission barriers.

	Fixed $\mathfrak{I}$			Spin-dependent $\mathfrak{I}$		
Z_{IMF}	B_{fiss}^{CN} (MeV)	J_{rms} (MeV)	$\frac{a_f}{a_n}$ (MeV)	B_{fiss}^{CN} ($\hbar$)	J_{rms} (MeV)	$\frac{a_f}{a_n}$ ($\hbar$)
4	35.0	63	1.097	35.7	65	1.097
5	36.7	66	1.094	36.7	66	1.097
6	35.5	67	1.091	35.5	67	1.097
7	38.7	68	1.091	37.7	67	1.093
8	40.0	69	1.091	38.5	67	1.093
9	42.7	69	1.091	40.7	67	1.093
10	42.5	70	1.091	39.7	68	1.091
11	42.7	70	1.088	39.7	70	1.087
12	42.2	70	1.084	38.7	70	1.084
13	42.5	71	1.084	39.0	71	1.085
14	42.1	71	1.083	38.0	71	1.083
15	42.2	71	1.081	38.0	71	1.082

Note that the calculated barriers vary smoothly with the asymmetry parameter, whereas those derived from the excitation functions show fluctuations in the relative yields. The implications of these fluctuations are discussed in Appendix A. The main point is that the barriers shown in Fig. 5 are on average $\approx$ 37% greater than those calculated by the YEFRN model; they also seem to be $\approx$ 10% smaller than those from the RLDM. In Appendix B we show that the YEFRN barriers do not give a satisfying result even if one varies the relevant spin zone for IMF emission.

This result differs dramatically from the results for ^{75}Br* reported in [9] where good agreement was found between the calculated YEFRN barriers and those extracted from the IMF excitation functions. For the ^{149}Tb* nucleus the YEFRN model seems to underestimate the barriers, possibly by overestimating the stabilization due to the nuclear force. In Ref. [10] Sierk has emphasized that the empirical footing is rather weak for

several empirical parameters (a_s and κ_s) in his formulation.

In all cases the derived ratios for the level density parameters (a_f/a_n in Table I) are greater than 1 for ^{149}Tb*. Values less than 1 were reported in a similar analysis for the system ^{75}Br* [9]. However, we note that in [9] ^{4}He emission was not considered, even though its cross sections are known to be important [19]. The good agreement reported in [9] between the derived IMF barriers and those calculated by the YEFRN model may be changed by inclusion of light-charged particle competition, which would presumably lower the IMF barriers extracted from the excitation functions. Conversely, an increase in the a_f/a_n ratios (perhaps to values $\geq$ 1) could enhance IMF competition with the opposite effect. It is likely that one would need to change both parameters in a re-analysis to obtain fits to the measured IMF yields. At this point it seems to us to be a moot point whether or not the IMF barriers for ^{75}Br* are in good agreement with YEFRN calculations.

Values extracted for J_{rms} are shown in the fifth column of Table I. Note that these values of J_{rms} increase with increasing Z as the fragment approaches the condition for symmetric fission. Indeed, the large values for J_{rms} for the heavier IMF's suggest that these fragments might well be considered a part of the exit channel process commonly called symmetric fission. The kinematics of recoil from such heavy IMF's would also remove the heavy recoil from the ER reaction group.
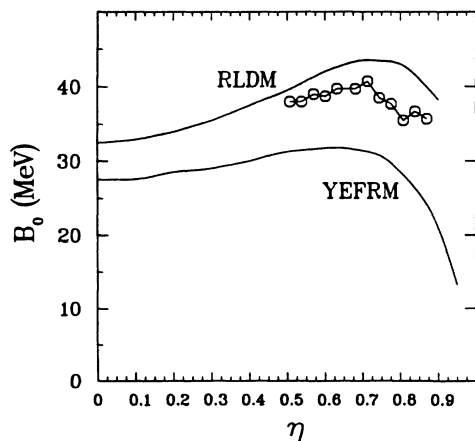

FIG. 5. Comparison of experimentally derived barriers (Table I, right-hand group) with YEFRN and RLDM predictions as functions of the asymmetry parameter η. Barrier values from the data were extracted with the use of moments of inertia from the YEFRN model. This gives a small inconsistency in their comparison to RLDM, but it is given here as a point of reference.

IV. DISCUSSION OF THE MODEL ASSUMPTIONS

To clarify this apparent discrepancy between the model predictions and the barrier values derived from the excitation functions, one must first reexamine the assumptions employed in the fitting procedure described above. In our most simple approach three assumptions have been made: (1) The barriers are not strongly influenced by the spin dependence of the moments of inertia for saddle-point nuclei. (2) Multiple-chance fission does not play

an important role in the results. (3) The spin range ($0\hbar$–$75\hbar$) is predominantly responsible for the production of the lighter IMF's, and thus these IMF's are mainly in competition only with light particles. Each of these assumptions is addressed below.

A. Spin-dependent moments of inertia

The YEFRN model predicts moments of inertia for saddle-point nuclei as a function of the angular momentum and the mass-asymmetry coordinate η of the system [13]. These spin-dependent moments of inertia have been incorporated into a second-level statistical model analysis of these excitation functions. The results of this second analysis are listed in the final three columns of Table I under the label "Spin dependent $\Im$." We see that for this analysis the extracted barriers are indeed smaller but still leave a significant gap to the model predictions (Fig. 5). Spin-dependent moments of inertia, however, seem to be preferable because they are better grounded in the framework of the model. Our conclusion, on the inadequacy of the standard approach, however, is independent of this choice.

B. Multiple-chance fission

In this section we develop a semiquantitative feeling for the relative importance of IMF emission after successive evaporation steps. Figure 6 shows calculated branching ratios for $Z = 10$ versus angular momentum for three different excitation energies: 194 MeV (the initial excitation energy for 640 MeV ^{86}Kr + ^{63}Cu), 176 MeV, and 158 MeV. These excitation energies are separated by 18 MeV, the average excitation energy removed from the composite nucleus by the evaporation of one ^{4}He. Within the

FIG. 6. Branching ratios for first-, second-, and third-chance fission for $Z = 10$ from ^{149}Tb* at an initial-excitation energy of 194 MeV.

framework of the statistical model, ^{4}He is expected to be the major ejectile from nuclei with higher spins [20,21] and thus in the competition with IMF emission. The average spin removed by each ^{4}He is $\approx 7\hbar$; hence we estimate that ≈ 7 units of angular momentum are removed from the emitter by the particle evaporation that competes with IMF emission. The ratio of the second-chance to first-chance emission can be estimated from the curves shown in Fig. 6, as described below.

For example, we see from Table I that for $Z = 10$, J_{rms} is $68\hbar$ (spin-dependent moment of inertia). The branching ratio for first-chance IMF emission ($E^* = 194$ MeV) is 0.075. Now suppose one ^{4}He is emitted and removes $7\hbar$ of spin and 18 MeV of excitation energy. The average residual nucleus is left with an excitation energy of 176 MeV and a spin of $61\hbar$. For this excitation energy, a new branching ratio of 0.021 can be taken from Fig. 6 for second-chance emission, i.e., 28% of the first-chance value. The third-chance probability is even less. We can say for the 640 MeV ^{86}Kr reaction, first-chance IMF emission constitutes $\approx 70\%$ of the total IMF cross section for $Z = 10$.

This procedure for estimating the first-chance IMF cross section may be extended to the other excitation energies for which IMF cross sections have been measured. We assume that the values of J_{rms} for first-chance emission are the same as those listed in Table I. For example, the first-chance emission cross section for carbon ranged from a low of 80% of the total (for $E^* = 231$ MeV) to a high of 92% (for $E^* = 128$ MeV). In this manner excitation functions for first-chance emission were approximated by subtracting off the estimated second- and third-chance cross sections from the total cross sections. These first-chance excitation functions were then fitted with the statistical model prescription described above. The extracted barriers were essentially unchanged (typically lower by ≤ 0.5 MeV) from the values listed in Table I. The value of J_{rms} also experiences a negligible change. In summary, the consideration of multiple-chance fission within the limits of this simple approximation does not significantly alter the derived fission barriers or the values of J_{rms}.

One should note, however, that Eq. (2.7) (used to calculate the IMF branching ratios) is formulated with respect to competition between IMF's and neutrons, not IMF's and ^{4}He. As noted previously, for the reactions studied here, neutron emission comprises $\approx 75\%$ of light particle emission, and therefore $\approx 75\%$ of the total level width [see Eq. (2.6)]. This value of 75% is therefore the probability for the emission of a neutron averaged over the entire ER spin range. The statistical model calculations shown in Fig. 5 and reported in Table I use this average and do not include more detailed information on the spin-dependent branching ratios which are expected to be enhanced for ^{4}He emission at high spins [20,21].

In principle, the statistical model code GEMINI treats the spin-dependent competition between all the exit channels over the entire deexcitation chain. This means that multiple-chance fission is directly handled by the code in a more complete fashion than in the method adopted above and in [9]. GEMINI also employs the Sierk
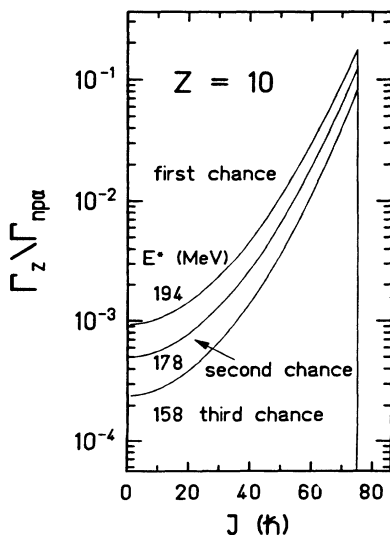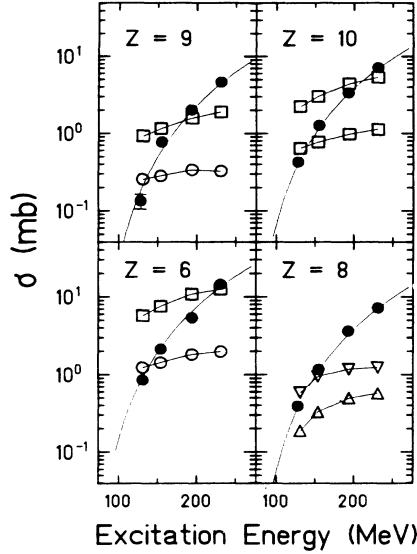
FIG. 7. Comparison of experimental IMF excitation functions (solid circles) with statistical model calculations made by GEMINI for $Z = 6,9$, and 10 with $J_{max} = 75$ and a_f/a_n equal to 1.0 (open circles) and 1.1 (open squares). For $Z = 8$ the GEMINI calculations are shown for $a_f/a_n = 1.0$ and $J_{max} = 60\hbar$ ($\triangle$), and $J_{max} = 80\hbar$ (∇). Lines drawn between calculated or measured yields are to guide the eye.

barriers in its calculations of the branching ratios, so that a comparison of the data to the IMF yields as calculated by GEMINI gives an additional test of these barriers. Figure 7 shows a comparison of experimental IMF yields for $Z = 6$, 9, and 10 (solid circles) with those calculated by GEMINI with spin range $0\hbar$–$75\hbar$ for two values of a_f/a_n: i.e., 1.0 (open circles) and 1.1 (open squares). For both values of a_f/a_n, the excitation functions calculated by GEMINI fail to reproduce both the absolute and relative IMF cross sections. The experimental excitation functions show steep slopes that GEMINI fails to duplicate. This problem cannot be cured by changing the spin zone as shown by the calculations in Fig. 7 for $Z = 8$. In other words, the YEFRN barriers, as incorporated in this code, do not account for the data.

With the simple framework of Eqs. (2.1)–(2.12) one can obtain smooth curves through the experimental points. The slope is very sensitive to the value of a_f/a_n; the larger this ratio, the steeper the slope. Values of a_f/a_n greater than 1 have the effect of increasing the partial width for IMF emission as a function of the excitation energy, thereby enhancing the IMF cross sections as a function of excitation energy. The slopes of the excitation functions as calculated by GEMINI appear to have little or no sensitivity to a_f/a_n, only an overall enhancement in the size of the calculated cross sections. In short, if one employs the YEFRN barriers, neither the standard simple procedure [9] nor the more detailed statistical model calculation from GEMINI is able to provide a satisfying description of the yields and excitation functions.

C. Competition with light particles

The third approximation of this analysis is that the IMF's are produced in competition with light particle

emission in the ER spin range. As discussed above we can be confident that most light IMF's are indeed associated with the ER reaction group. The calculations shown in Fig. 3, e.g., indicate a significant but decreasing contribution for fission below the empirical sharp cutoff value of $75\hbar$. In the approach used here one is assigning to IMF production that part of the overall fission process which occurs for $J \leq 75\hbar$. In this way one is consistent in the statistical model treatment of competition between light particles and IMF's (the latter being themselves the relevant fission fragments produced for $J \leq 75\hbar$). For composite nuclei with spins $\geq 75\hbar$, the fission barrier is expected to vanish and serious calculations for fragment production will require a full dynamical model. Such calculations are beyond the scope of this work.

In addition to the above considerations of spin-dependent moments of inertia, multiple-chance fission, and competition with light particles, the IMF excitation functions have been fitted with the Sierk barriers by using the spin range as a fitting parameter. This approach has been adopted to test whether a reasonable spin range along with the Sierk barriers could be consistent with the IMF yields. As discussed in Appendix B, the derived spin range is much too narrow to be believable.

V. SUMMARY AND CONCLUSIONS

Asymmetric fission barriers have been obtained from an empirical analysis of IMF excitation functions. The spin range employed in these calculations ^{149}Tb* was taken to be $0\hbar$–$75\hbar$ as inferred from the cross section for ER's. We make the following observations and conclusions.

(1) Values of the asymmetric fission barriers derived from the IMF excitation functions are significantly larger than those predicted by the YEFRN model. It would appear that the YEFRN model underestimates the barriers by overestimating the stabilization due to the nuclear force via some of the empirical parameters in the model.

(2) Previous work [9] claims agreement between empirical IMF barriers for ^{75}Br* and the calculated YEFRN model. This very similar analysis of the IMF excitation functions did not include ^{4}He competition in the statistical model calculations. Such additional competition might well change the extracted barriers and the values of a_f/a_n in order to maintain the good fits to the IMF excitation functions, but this should be reexamined.

(3) The statistical model code GEMINI, with YEFRN barriers, fails to account for the IMF excitation functions.

ACKNOWLEDGMENTS

APPENDIX A: FINE STRUCTURE AND SHELL EFFECTS

One should note that the extracted barriers in Fig. 5 do not vary smoothly with mass asymmetry parameter. Carbon has the lowest barrier, which follows from its large cross sections; fluorine, on the other hand, has the largest barrier. Barriers calculated from the RLDM and YEFRN model vary smoothly with asymmetry parameter because these models assume a continuous mass distribution of uniform charge to mass ratio. By contrast, these experimental cross sections and many others (e.g., [22]) seem to reflect "shell or pairing effects"that are observed as fine structure in the IMF charge distribution.

These cross section irregularities suggest that the binding energies of the fragments themselves, and not just the barriers, play a role in driving the IMF yields, at least for the lighter IMF's ($Z \leq 9$). This fact suggests that the primary IMF yields are frozen in at configurations that possess final-fragment character, e.g., somewhere between the saddle and scission points. This seems to be the case also for fixation of the total kinetic energy released in fission [2,13,17]. The combined observations of pre-scission emission of ^{4}He [5,20,21], large pre-scission neutron multiplicities [23,24], and high-energy γ rays [25] strongly indicate that the fission process does indeed proceed slowly, giving time for the possibility of nucleon exchange in the descent from saddle to scission points. In this context, an emerging fragment with an even Z may be less inclined to surrender a proton to its partner than a developing fragment of odd Z. Presumably the closer the nucleus is to the scission point, the stronger is the role of these pairing and/or shell effects. If the IMF yields are not frozen in at the saddle point, as these fluctuations suggest, then we should remain critical of the concept of a preeminent role of the saddle-point nucleus in statistical model predictions [i.e., Eq. (2.3)].

APPENDIX B: AN ANALYSIS THAT ASSUMES VALIDITY OF YEFRN BARRIER VALUES

Experimental IMF cross sections may often be fitted by using YEFRN model barriers if the spin range of the emitters is taken as a free parameter. Here we give a statistical model analysis using barrier values taken from the YEFRN model; they are $\approx$ 37% smaller than the empirical set in Table I. These lower barriers generate much larger calculated IMF cross sections, which call

TABLE II. Asymmetric fission barriers that match YEFRN barriers.

Z_{IMF}	YEFRN	J_{rms}	J_{max}	a_f/a_n
4	23.4	4	6	1.153
5	25.6	7	10	1.150
6	27.7	28	36	1.118
7	29.0	25	33	1.117
8	30.0	30	38	1.116
9	30.6	25	32	1.118
10	31.0	32	40	1.115
11	31.7	42	49	1.100
12	31.7	49	55	1.090
13	31.6	49	55	1.090
14	31.5	51	57	1.090
15	31.5	53	59	1.085

for smaller values of the maximum emitter spin. Indeed production of IMF's is much less competitive with light particle production at lower spins, as shown in Fig. 1; therefore a reduction in the allowed spin range will lead to a strong nonlinear reduction in the calculated cross sections. With this approach, fits to the excitation functions can be obtained that are almost identical to those shown in Fig. 4. Upper limits to the spin ranges used for these fits (J_{max}) as well as the values of J_{rms} and a_f/a_n are listed in Table II.

This analysis requires a dramatic reduction in the allowed spin zone, i.e., the J_{max} values in Table II are all significantly smaller than $75\hbar$, the empirical value for ER production. It is difficult to imagine a justification for such a restricted spin range. The qualitative trends shown in Figs. 1–3 would have to be arbitrarily rejected. Furthermore, such low spins are not easily reconciled with the large observed anisotropies in the IMF angular distributions [5]. The anisotropies for the IMF's are larger than those measured for ^{4}He from the same reactions [5,17] and appear to follow a nearly $1/\sin\theta_{c.m.}$ angular dependence, the classical limit for emission from a nucleus with a large angular momentum. In short, it does not seem plausible to conclude that only a low-spin portion of the ER spin range is responsible for IMF production.

An additional attempt has been made to reproduce the experimental cross sections and YEFRN model barriers while at the same time retaining $75\hbar$ as the maximum angular momentum. In this procedure we varied the ratio of level density parameters a_f/a_n employed. However, no single value of this ratio is able to reproduce a given IMF yield over the studied range.

[1] V. E. Viola, J. L. Wile, D. E. Fields, K. Kwiatkowski, S. J. Yennello, H. M. Xu, M. B. Tsang, R. T. deSouza, E. Renshaw, J. Pochodzalla, K. B. Morely, W. G. Lynch, W. G. Gong, C. K. Gelbke, D. J. Fields, and N. Carlin, Nucl. Phys. A538, 291c (1992).

[2] J. Boger, S. Kox, G. Auger, J. M. Alexander, A. Narayanan, M. A. McMahan, D. J. Moses, M. Kaplan, and G. P. Gilfoyle, Phys. Rev. 41, R801 (1990).

[3] R. Trockel, K. D. Hildenbrand, U. Lynen, W. F. J.

Mueller, H. J. Rabe, H. Sann, H. Stelzer, W. Trautmann, R. Wada, E. Eckert, P. Kreutz, A. Kuehmichel, J. Pochodzalla, and D. Pelte, Phys. Rev. C 39, 729 (1989).

[4] Y. Cassagnou, M. Conjeaud, R. Dayras, S. Harar, G. Klotz-Engmann, R. Legrain, V. Lips, H. Oeschler, E. C. Pollaco, and C. Volant, in Nuclear Dynamics and Nuclear Disassembly—1989 Dallas, Texas, edited by J. B. Natowitz (World Scientific, Singapore, 1989), p. 386.

[5] J. Boger, J. M. Alexander, A. Elmaani, S. Kox, R. A.

Lacey, A. Narayanan, D. J. Moses, M. A. McMahan, P. A. DeYoung, and C. J. Gelderloos, Phys. Rev. C **49**, 1597 (1994).

[6] L. G. Sobotka, M. L. Padgett, G. J. Wozniak, G. Guarino, A. J. Pacheco, L. G. Moretto, Y. Chan, R. G. Stokstad, I. Tserruya, and S. Wald, Phys. Rev. Lett. **51**, 2187 (1983).

[7] R. J. Charity, D. R. Bowman, Z. H. Liu, R. J. McDonald, M. A. McMahan, G. J Wozniak, L. G. Moretto, S. Bradley, W. L. Kehoe, and A. C. Mignerey, Nucl. Phys. **A476**, 516 (1988).

[8] M. A. McMahan, L. G. Moretto, M. L. Padgett, G. J. Wozniak, L. G. Sobotka, and M. G. Mustafa, Phys. Rev. Lett. **54**, 1985 (1985).

[9] D. N. Delis, Y. Blumenfeld, D. R. Bowman, N. Colonna, K. Hanold, K. Jing, M. Justice, J. C. Meng, G. F. Peaslee, G. J. Wozniak, and L. G. Morretto, Z. Phys. A **339**, 279 (1991).

[10] A. J. Sierk, Phys. Rev. Lett. **55**, 582 (1985); Phys. Rev. C **33**, 2039 (1986).

[11] H. J. Krappe, J. R. Nix, and A. J. Sierk, Phys. Rev. C **20**, 992 (1979).

[12] S. Cohen, F. Plasil, and W. J. Swiatecki, Ann. Phys. (N.Y.) **82**, 557 (1974).

[13] N. Carjan and M. Kaplan, Phys. Rev. C **45**, 2185 (1992); N. Carjan and J. M. Alexander, *ibid.* **38**, 1692 (1988).

[14] R. Vandenbosch and J. R. Huizenga, *Nuclear Fission* (Academic, New York, 1973), Chaps. 7 and 8.

[15] L. C. Vaz, D. Logan, J. M. Alexander, E. Duek, D. Guerreau, L. Kowalski, M. F. Rivet, and M. S. Zisman, Z.

Phys. A **311**, 89 (1983).

[16] E. Puehlhofer, Nucl. Phys. **A213**, 267 (1977).

[17] J. Boger, J. M. Alexander, G. Auger, A. Elmaani, S. Kox, R. A. Lacey, A. Narayanan, M. Kaplan, D. J. Moses, M. A. McMahan, P. A. DeYoung, C. J. Gelderloos, and G. Gilfoyle, Phys. Rev. C **49**, 1576 (1994); J. Boger, Ph.D. thesis, SUNY Stony Brook, 1992.

[18] N. Carjan, H. Delagrange, and A. Fleury, Phys. Rev. C **19**, 2267 (1979).

[19] R. C. Reedy, M. J. Fluss, G. F. Herzog, L. Kowalski, and J. M. Miller, Phys. Rev. **188**, 1771 (1969).

[20] R. Lacey, N. N. Ajitanand, J. M. Alexander, D. M. de Castro Rizzo, G. F. Peaslee, L. C. Vaz, M. Kaplan, M. Kildir, G. La Rana, D. J. Moses, W. E. Parker, D. Logan, M. S. Zisman, P. DeYoung, and L. Kowalski, Phys. Rev. C **37**, 2561 (1988).

[21] W. E. Parker, M. Kaplan, D. J. Moses, J . M. Alexander, J. T. Boger, R. A. Lacey, and D. M. de Castro Rizzo, Nucl. Phys. **A568**, 633 (1994).

[22] L. G. Moretto and G. J. Wozniak, Prog. Part. Nucl. Phys. **21**, 401 (1988).

[23] A. Gavron, A. Gayer, J. Boissevain, H. C. Britt, T.C. Awes, J. R. Beene, B. Cheynis, D. Drain, R. L. Ferguson, F. E. Obenshain, F. Plasil, G. R. Young, G. A. Petitt, and C. Butler, Phys. Rev. C **35**, 579 (1987).

[24] D. J. Hinde, D. Hilscher, H. Rossner, B. Gebauer, M. Lehmann, and M. Wilpert, Phys. Rev. C **45**, 1229 (1992).

[25] D. J. Hoffman, B. B. Back, I. Dioszegi, C. P. Montoya, S. Schadmand, R. Varma, and P. Paul, Phys. Rev. Lett. **72**, 470 (1994).